ChemPhysChem

Research Article
doi.org/10.1002/cphc.202300305

Chemistry Europe
European Chemical
Societies Publishing

www.chemphyschem.org

Resonant Fragmentation of the Water Cation by Electron Impact: a Wave-Packet Study

Ignacio Benito-Gómez+,[a] Luis Méndez+,[a] Jaime Suárez+,[a] Jimena D. Gorfinkiel+,[b] and Ismanuel Rabadán+*[a]

We have investigated the dissociation of a resonant state that can be formed in low energy electron scattering from H_2O^+. We have chosen the second triplet resonance above the $\tilde{B}\,^2A'$ ($\tilde{B}\,^2B_2$) state of H_2O^+ whose autoionization mainly produces H_2O^+ ($\tilde{X}\,^2A''$). We have considered both dissociation of the resonant state itself, dissociative recombination (DR), or the dissociation of the H_2O^+ cation after autodetachment, dissociative excitation (DE). The time-evolution of a wave packet on the potential energy surfaces of the resonance and cationic states shows, for the initial conditions studied, that the probability for DR is about 38% while the probability for DE is negligible.
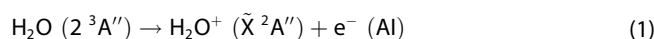
Introduction

Low-energy electron collisions with singly-charged molecular cations can lead to the formation of many molecular resonant states embedded in one or several electronic and vibrational continua. These resonance states will evolve, leading to several possible products that depend on their autoionization lifetimes, dissociation times, etc. One can model this by following the evolution of a nuclear wave-packet on the resonance potential energy surface until it either emits one electron, leaving behind a molecular cation, or fragments into neutral products; the latter process is called dissociative recombination (DR). Depending on the amount of electronic energy transformed into nuclear kinetic energy, the molecular cation left behind by autoionization can fragment, a process known as dissociative excitation (DE), or just remain vibrationally excited.
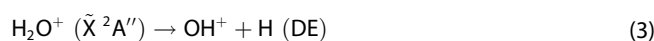
DR and DE reactions in electron collisions with H_2O^+ are relevant in radiation damage of biological systems, where the ionization of water molecules produces electrons that, in a second stage, can yield highly reactive OH radicals, which damage the DNA through different mechanisms reviewed by Dizdaroglu and Jaruga.[1] OH radicals are also important in the Earth's atmosphere, where they clean the air by breaking down organic molecules. DR and DE in electron collisions with H_2O^+

[a] I. Benito-Gómez,+ Prof. L. Méndez,+ Dr. J. Suárez,+ Dr. I. Rabadán+
Laboratorio Asociado al CIEMAT de Física Atómica y Molecular en Plasmas de Fusión, Departamento de Química, módulo 13,
Universidad Autónoma de Madrid
28049 Madrid, Spain
E-mail: ismanuel.rabadan@uam.es
Homepage: https://portalcientifico.uam.es/es/ipublic/researcher/260037

[b] Prof. J. D. Gorfinkiel+
School of Physical Sciences, The Open University, Walton Hall
MK7 6AA Milton Keynes, UK

[+] These authors contributed equally.

were studied in the ASTRID experiment of Jensen et al.[2] In addition, DR was also investigated by Mul et al.[3] and in CRYRING experiments[4–6] and DE by Fogle et al.[7] The theoretical works are scarce: Nkambule et al.[8] studied DR, and, more recently, Rabadán and Gorfinkiel[9] carried out R-matrix calculations[10] to characterize resonant states with energies of up to 13 eV above the $\tilde{X}\,^2A''$ ($\tilde{X}\,^2B_1$ in C_{2v} symmetry) state of H_2O^+ at its equilibrium geometry. Molecular resonant states in that energy range include the complete Rydberg series converging to the $\tilde{A}\,^2A'$ ($\tilde{A}\,^2A_1$) and $\tilde{B}\,^2A'$ ($\tilde{B}\,^2B_2$) of H_2O^+ and the low members of the Rydberg series converging to the dissociative cation states $\tilde{C}\,^2A''$ ($\tilde{C}\,^2A_1$), $\tilde{a}\,^4A''$ ($\tilde{a}\,^4B_1$) and $\tilde{D}\,^2A'$ ($\tilde{D}\,^2A_1$). The aim of their work was to investigate the characteristics of these resonances and determine the likelihood of them having a significant effect on the DE process in the 5–10 eV energy range. They produced resonance data that can be used in calculations that included the nuclear degrees of freedom.

In this work, we study the competition between DR and DE in the dynamics of one of the above-mentioned resonant states of H_2O, specifically the second triplet resonant state above the $\tilde{B}\,^2A'$ ($\tilde{B}\,^2B_2$) of H_2O^+, labelled $2\,^3A''$ ($2\,^3A_2$ in C_{2v} symmetry) by Rabadán and Gorfinkiel, whose parent ion state is $\tilde{C}\,^2A''$. Schematically, we start with a nuclear wave packet corresponding to the ground vibrational state of the H_2O^+ cation in its ground electronic state $\tilde{X}\,^2A''$. The colliding electron is captured by the molecular cation to form the resonant state of H_2O ($2\,^3A''$), whose main[9] autoionization (AI) channel is the $\tilde{X}\,^2A''$ state. Therefore, the resonant state can decay through the reactions:
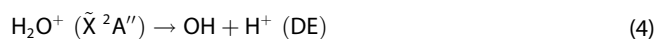
$$H_2O\ (2\,^3A'') \rightarrow H_2O^+\ (\tilde{X}\,^2A'') + e^-\ \text{(AI)} \tag{1}$$

$$H_2O\ (2\,^3A'') \rightarrow OH + H\ \text{(DR)} \tag{2}$$

The cation produced in Eq. (1) can dissociate through the reactions:

$$H_2O^+\ (\tilde{X}\,^2A'') \rightarrow OH^+ + H\ \text{(DE)} \tag{3}$$

ChemPhysChem

Research Article
doi.org/10.1002/cphc.202300305

Chemistry Europe
European Chemical
Societies Publishing

$$H_2O^+ \ (\tilde{X} \ ^2A'') \rightarrow OH + H^+ \ (DE) \qquad (4)$$

where the DE process that yields $OH + H^+$ requires the population of the $\tilde{A} \ ^2A'$ state from $\tilde{X} \ ^2A''$ through a Renner–Teller coupling at linear geometries.[11]

In the present work, we have carried out a wave packet (WP) simulation to determine the probabilities of dissociation in the two potential energy surfaces PESs (2 $^3A''$ and $\tilde{X} \ ^2A''$). The calculation is based on the works of Suarez *et al.*[11,12] on fragmentation on H_2O^+, where the time-dependent Schrödinger equation (TDSE) is solved numerically using a lattice method. A summary of the method is presented in section Computational Method, where we also consider the modifications required to deal with non-stationary states. In section Results and Discussion we present the results of the simulation, and the main conclusions are outlined in section Conclusion. Atomic units are employed unless otherwise stated.

Computational Method

In our calculation, the nuclear wavefunction is solution of the TDSE in the body-fixed reference frame, employing the non-rotating ($J = 0$) Hamiltonian. It is convenient to write the Hamiltonian (see e.g. Leforestier)[13] in terms of the Jacobi coordinates $\{r, R, \theta\}$, shown in Figure 1, where r is the vector from the O nucleus to one of the hydrogen nuclei; R is the vector from the center of mass of the system O−H to the second hydrogen, and θ is the angle between the vectors R and r.

In the lattice method, the WP is the solution of the matrix equation:

$$i\dot{\Psi} = H\Psi = (T + V)\Psi, \qquad (5)$$

where the vector Ψ stores the values of the WP, Ψ, at points of a 3D grid, and $\dot{\Psi}$ is the time-derivative of Ψ. We assume that the resonant state 2 $^3A''$ is formed in an electron collision with the ground vibronic state of H_2O^+, and that the electron attachment is a fast process that takes place without changing the nuclear wavefunction. Hence, the propagation starts from the ground vibrational wavefunction of H_2O^+, which will evolve on the resonant PES 2 $^3A''$. Autoionization mainly yields transitions from H_2O (2 $^3A''$) to H_2O^+ ($\tilde{X} \ ^2A''$). Therefore, the calculation must include these transitions, and the vibrational WP moves on two PESs, those of 2 $^3A''$, Ψ_{res}, and $\tilde{X} \ ^2A''$, $\Psi_{\tilde{X}}$. We have:

$$\Psi = \begin{pmatrix} \Psi_{res} \\ \Psi_{\tilde{X}} \end{pmatrix}, \qquad (6)$$

From this, the probability densities on both components are $P_{res} = |\Psi_{res}|^2$ and $P_{\tilde{X}} = |\Psi_{\tilde{X}}|^2$.

In this two-state simulation, the potential energy matrix, V, is diagonal; it stores the PESs calculated at the grid points. Since we consider electronic states of the neutral molecule and the cation, the non-adiabatic couplings between the two electronic states vanish, and it is not necessary to perform an adiabatic-to-diabatic transformation that would introduce off-diagonal matrix elements in V. To describe the autoionization, the potential energies of 2 $^3A''$ determined in the R-matrix calculations[9] have an imaginary part related to the resonance lifetime.
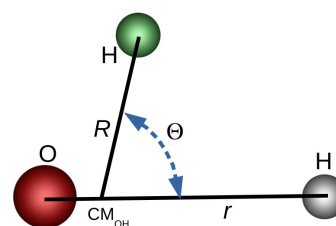

Figure 1. Jacobi coordinates employed to study the H_2O molecule.

The matrix T of Eq. (5) includes the kinetic energy matrix elements obtained by means of a finite differences method.[14] In practice we have used a 15-point stencil; it yields a highly sparse matrix, allowing an efficient parallelization of the GridTDSE[15] code.

The WP simulation has been carried out employing the GridTDSE code of Suarez *et al.*,[15] modified to incorporate transitions between several PESs.[12] In the present calculation, the nuclear WP is propagated on two adiabatic PESs. The dynamical calculation employs a grid of 484720 nuclear configurations defined in the Jacobi coordinates $\{R, r, \theta\}$; the grid includes points generated from 83 values for $R \in [1.0; 11.0]$ bohr, 80 values for $r \in [1.3; 11.0]$ bohr and 73 values for $\theta \in [0.004; 3.137592]$ rad. The electronic energies of H_2O^+ ($\tilde{X} \ ^2A''$) in this grid were calculated by Suarez *et al.*,[11] using a multireference configuration interaction method (MRCI), with MOLPRO.[16] For the MRCI wave functions, configurations were generated by distributing seven electrons in the active space consisting of seven a′ and one a″ molecular orbitals. These orbitals were obtained from a complete-active-space self-consistent-field (CASSCF) calculation using the basis sets aug-cc-pVQZ and aug-cc-pVTZ for oxygen and hydrogen respectively, and an active space with 10 a′ and one a″ orbitals.

In the simulation, the electronic energy of the resonant state 2 $^3A''$ has been approximated by shifting that of the parent state of H_2O^+ ($\tilde{C} \ ^2A''$) by -0.2 hartree. This was determined to be a good approximation[9] to the resonant PES obtained from the R-matrix calculations using the UKRmol+ suite.[17] This approximation is, in general, valid, except for some regions where the $\tilde{C} \ ^2A''$ PES exhibits avoided crossings with other states of H_2O^+. Cuts of the PESs for the H_2O^+ ($\tilde{X} \ ^2A''$) equilibrium geometry, $\{r_0, \theta_0\}$ and $\{r_0, R_0\}$, are shown in Figures 2 and 3, respectively.
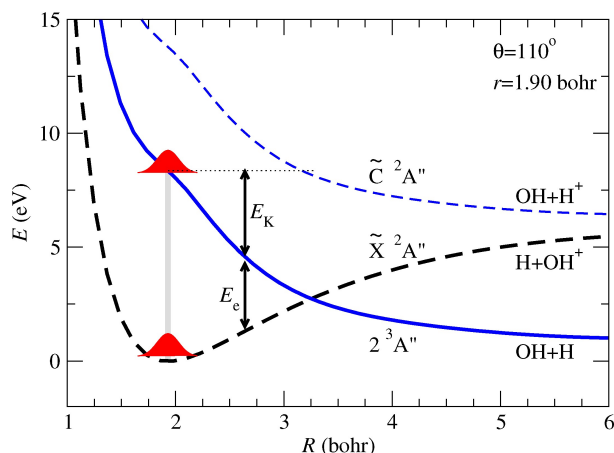
The time-evolution of the WP is obtained by solving Eq. (5) with a second-order differences method:

$$\Psi(t + \Delta t) = \Psi(t - \Delta t) - 2i\Delta t \hat{H}\Psi(t) \qquad (7)$$

In our calculations, $\Delta t = 7.5 \times 10^{-3}$ a.u. ($\equiv 1.8 \times 10^{-3}$ fs). It is worth noting that the second order differences method conserves norm and energy of the WP.[18,19]

As in previous applications,[11] we have included a damping function[20] in the propagation scheme to avoid unphysical reflections of the wave function at the grid walls ($L_{max} = 11$ bohr). This function leads to a smooth decay of the wave packet for and is defined as:

$$M(q) = \begin{cases} e^{-\xi(q - L_{max} + \delta)^2} & \text{if } q < L_{max} - \delta \text{ elsewhere,} \\ 1 \end{cases} \qquad (8)$$

ChemPhysChem

Research Article
doi.org/10.1002/cphc.202300305

Chemistry Europe
European Chemical
Societies Publishing

Figure 2. Cut of the potential energy surfaces of the $\tilde{X}\,^2A''$ and $\tilde{C}\,^2A''$ states of H_2O^+ (dashed-lines) and the $2\,^3A''$ resonant state (solid line) of H_2O along the coordinate R, with $r = 1.90$ bohr and $\theta = 110°$. Asymptotic fragments are indicated next to the curves. The initial WP is sketched to illustrate the mechanisms of DR and DE reactions. E_K is the kinetic energy the WP gains, while E_e is the maximum kinetic energy of the electron emitted by autoionization.
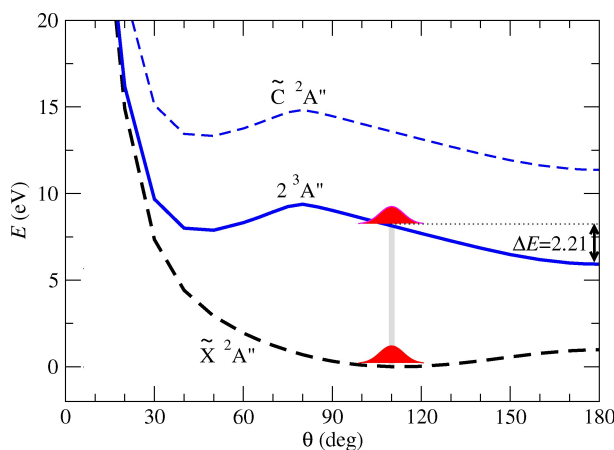
Figure 3. Cut of the potential energy surfaces of the $\tilde{X}\,^2A''$ and $\tilde{C}\,^2A''$ states of H_2O^+ and the $2\,^3A''$ resonant state of H_2O along the coordinate θ, with $R = 1.979$ bohr, and $r = 1.90$ bohr. ΔE is the maximum electronic energy transfered into the bending degree of freedom.

with $q \equiv (R, r)$, $\delta = 1$ bohr and $\xi = 0.05$ bohr^{-2}. The fragmentation is described numerically by the probability lost at the borders of the box due to the presence of the damping function.

As mentioned above, the autoionizing character of resonance $2\,^3A''$ is described by an imaginary energy related to its resonance width Γ:

$$E_{res} = \begin{cases} E_{res}^0 - \dfrac{i}{2}\Gamma & \text{if } R < 3.2 \text{ bohr or } r < 3.2 \text{ bohr} \\[2ex] E_{res}^0 & \text{if } R \geq 3.2 \text{ bohr or } r \geq 3.2 \text{ bohr.} \end{cases} \tag{9}$$

The cut-off in the imaginary part prevents the autoionization of $2\,^3A''$ when its energy falls below that of the cation ground state, which, we assume, takes place for $\{R,\ r\} \approx 3.2$ bohr.[9]

The width of $2\,^3A''$, $\Gamma(R, r)$, is related to the lifetime, τ, as $\Gamma = 1/\tau$. We have employed a Gaussian fitting of the data of $\tau(R,\ r)$ (Figure 7 of Rabadán and Gorfinkiel),[9] which yields, in atomic units:

$$\Gamma(R,\ r) = 1.06 \times 10^{-4}\, e^{0.24\left(R^2 + r^2\right)}, \tag{10}$$

The numerical differentiation method is also applied to calculate the probability density current. To calculate the probability lost on the grid borders, we have employed the two-component vectors:

$$\boldsymbol{j}_k = \frac{1}{2\mu_k}\left[\Psi^*\frac{\partial}{\partial q_k}\Psi - \left(\frac{\partial}{\partial q_k}\Psi^*\right)\Psi\right], \tag{11}$$

where:

$$\begin{aligned} q_1 &= r; & \mu_1^{-1} &= m_H^{-1} + m_O^{-1} \\ q_2 &= R; & \mu_2^{-1} &= m_H^{-1} + m_{OH}^{-1} \end{aligned} \tag{12}$$

and with $\Psi \equiv \Psi_{res}$ or $\Psi_{\tilde{X}}$.

The initial nuclear WP, $\Psi_{res}(r, R, \theta)$ is obtained[8,21–23] from the cation ground state, Φ, using the Lanczos method[24] and the numerical PES of $\tilde{X}\,^2A''$:

$$\Psi_{res} = \sqrt{\frac{\Gamma}{2\pi}}\Phi. \tag{13}$$

This WP evolves on the three coordinates of the $2\,^3A''$ PES, r, R, and θ (see Figure 2).

In practice, we have renormalized the WP and set the probability of finding the wavepacket on the resonance surface at $t = 0$: $P_{res}(t = 0) = \|\Psi_{res}(t = 0)\|^2 = 1$. At $t > 0$, the value of P_{res} decreases due to both autoionization, transferring probability to the cation state $\tilde{X}\,^2A''$, and the fragmentation of the WP into neutrals. One can write:

$$\frac{dP_{res}}{dt} = -\mathcal{A}(t) - \mathcal{F}_{res}(t), \tag{14}$$

where, $\mathcal{A}(t) = -\Gamma P_{res}$ corresponds to the autoionization process and $\mathcal{F}_{res}$ is the probability leak through the surface S defined by $R = r = L_{max}$:

$$\mathcal{F}_{res}(t) = \int_S \nabla \cdot \boldsymbol{j}_{res}, \tag{15}$$

where $\boldsymbol{j}_{res}$ is the probability density current (Eq. (11)) for the WP component Ψ_{res}.

The component $\Psi_{\tilde{X}}$ starts with value zero, and it increases with time through autoionization, but it can decrease via the cation fragmentation. The population of the WP $\Psi_{\tilde{X}}$ takes place through a sequence of incoherent transitions at points $t = t_1$. Analogously to Eq. (14), we write:

$$\frac{dP_{\tilde{X}, t_1}(t)}{dt} = \mathcal{A}(t)\delta(t - t_1) - \mathcal{F}_{\tilde{X}}(t), \tag{16}$$

where:

ChemPhysChem

Research Article
doi.org/10.1002/cphc.202300305

Chemistry
Europe
European Chemical
Societies Publishing

$$\mathcal{F}_{\tilde{X}}(t) = \int_s \nabla \cdot \boldsymbol{j}_{\tilde{X}}, \tag{17}$$

and $\boldsymbol{j}_{\tilde{X}}$ is the probability density current for dissociation in $\tilde{X}\ ^2A''$.

To describe the evolution of the WP on the $\tilde{X}\ ^2A''$ PES after a single event of autoionization of the resonant state at time t_1, we write:

$$\frac{d\Psi_{\tilde{X}}(t;\ t_1)}{dt} = \sqrt{\Gamma}\Psi_{res}(t)\delta(t - t_1) + i\boldsymbol{H}\Psi_{\tilde{X}}(t;\ t_1) \tag{18}$$

Here, if $t < t_1$, $\Psi_{\tilde{X}}(t;\ t_1) = 0$. The propagation of the WP on $\tilde{X}\ ^2A''$ is run for a collection of values of t_1 in the range $0.1\ \text{fs} < t_1 < 200\ \text{fs}$. Finally, the probability at time t of finding the system on the $\tilde{X}\ ^2A''$ PES is obtained from the incoherent superposition of the functions calculated by transitions at each value of t_1:

$$P_{\tilde{X}}(t) = \int_0^t ||\Psi_{\tilde{X}}(t;\ t_1)||^2 dt_1 = \int dV \rho_{\tilde{X}}(t;\ t_1) \tag{19}$$

with:

$$\rho_{\tilde{X}}(t) = \int_0^t |\Psi_{\tilde{X}}(t;\ t_1)|^2 dt_1. \tag{20}$$

We have also checked numerically that the probabilities of both states can be obtained in a single WP propagation where the $\Psi_{\tilde{X}}$ is continuously fed during the propagation:

$$\Psi_{\tilde{X}}(t + \delta) = \Psi_{\tilde{X}}(t) + a\Psi_{res}(t), \tag{21}$$

where Ψ_{res} comes from the evolution on the corresponding complex energy surface, and the parameter a is obtained by imposing the norm conservation:

$$P_{\tilde{X}}(t + \delta) + P_{res}(t + \delta) = P_{\tilde{X}}(t) + P_{res}(t) - F, \tag{22}$$

with F the probability lost by fragmentation in the time interval $[t,\ t + \delta]$. To order δ we obtain:

$$a = \frac{\langle\Psi_{res}|\Gamma|\Psi_{res}\rangle - F}{2Re\langle\Psi_{res}|\Psi_{\tilde{X}}\rangle}, \tag{23}$$

which, substituted in Eq. (21), leads to an expression that does not include interference terms between both WPs, showing that it is equivalent to the previously outlined non-coherent treatment.

Results and Discussion

The results of the WP simulation are illustrated in Figures 4 and 6. In Figure 4 we show the time-evolution of the probabilities P_{res} and $P_{\tilde{X}}$. In Figure 6 we display 2D cuts of the absolute values of the WPs $|\Psi_{res}(R, r_0, \theta;\ t)|$ and $[\rho_{\tilde{X}}(R, r_0, \theta;\ t)]^{1/2}$ [see Eq. (20)] for $r_0 = 1.90$ bohr. The color plots of the moduli of the WPs are drawn over the contour plots of the corresponding PESs also for $r = r_0$.

Initially, the WP moves on the $2\ ^3A''$ PES, and, as mentioned before, we have renormalized the initial WP and taken:
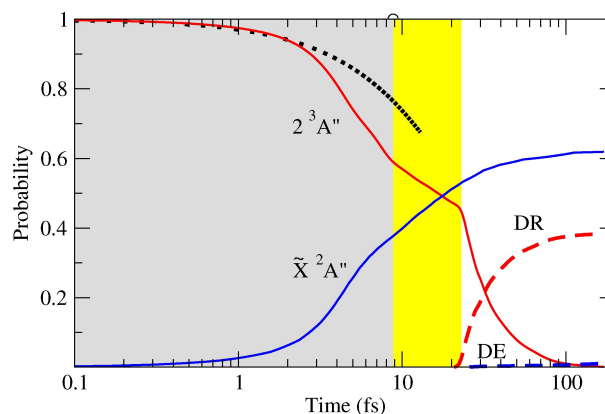
Figure 4. Time evolution of the probabilities P_{res} (solid red line) and $P_{\tilde{X}}$ (solid blue line). The dashed black line is the exponential decay $e^{-\gamma t}$ with $\gamma = 0.03\ \text{fs}^{-1}$. The dash-red line is the probability of fragmentation along the resonance channel, identified with DR. Fragmentation along the state of H_2O^+ is negligible and barely visible at the bottom of the graph (dashed-blue line). The three shaded regions correspond to different stages of the dynamics, as described in the text.

$$\begin{aligned} P_{res}(t = 0) &= \|\ \Psi_{res}(t = 0)\ \|^2 = 1 \\ P_{\tilde{X}}(t = 0) &= \|\ \Psi_{\tilde{X}}(t = 0)\ \|^2 = 0, \end{aligned} \tag{24}$$

which are the initial probabilities in Figure 4. We also illustrate the initial condition in the top-left panel of Figure 6.

The PES of state $2\ ^3A''$ is dissociative, as shown by the isolines in Figure 6 and the cuts along the R and θ coordinates of Figures 2 and 3. The WP experiences a strong gradient that moves it towards larger R; after 1.5 fs, its maximum has moved to $R \approx 2.1$ bohr. Simultaneously, the autoionization has transferred 4% of the probability to $\tilde{X}\ ^2A''$ (see Figure 4 and panels for $t = 1.5$ fs of Figure 6). At 3 fs, almost 12% of the probability is in the $\tilde{X}\ ^2A''$ state. For $t \lesssim 8$ fs, the probability P_{res} decays exponentially: the rate of autoionization increases as one or both OH bonds are elongated and the resonance lifetime decreases.

We can distinguish several stages during the molecular fragmentation. The gray region in Figure 4 covers the first 9 fs, while the WP moves towards larger values of R, r and θ, and autoionization is populating the $\tilde{X}\ ^2A''$ state. One can note in the isolines of Figure 6 and, more clearly, in Figure 3, that the energy of the resonant state decreases as θ increases. Therefore, the WP moves to larger θ, and, after 6 fs, it has reached $\theta = 180°$. P_{res} and $P_{\tilde{X}}$ show a noticeable change in slope at $t = 9$ fs, which initiates the yellow shaded region in the figure. For $t \geq 9$ fs, the WP spreads over a large region; in particular, part of the WP explores the region $R, r > 3.2$ bohr, where autoionization does not take place [see Eq. (9)]. This stage lasts up to about $t \approx 22$ fs, when fragmentation along the resonance starts. This indicates that the WP has arrived to the edge of the grid and the flux through this surface is accounted as fragmentation. For $t < 22$ fs, there is no fragmentation and the only process is the transfer of population from the resonance to the $\tilde{X}\ ^2A''$ state. For $t > 22$ fs, the WP is being absorbed by the damping function at the grid wall, representing DR or DE, depending on its channel components. Our simulation indicates

ChemPhysChem

Research Article
doi.org/10.1002/cphc.202300305

Chemistry Europe
European Chemical
Societies Publishing

that 38% of the initial WP ends up as fragmentation along the resonance, likely DR, while 62% remains in the $\tilde{X}\,^2A''$ state of the water cation.

The final results will not be substantially affected by the extension of the grid box. The increase of the box size will lead to an increase of the plateau region of $P_{res}(t)$ in Figure 4, but at the end of this region, at $t \approx 30$ fs, $P_{\tilde{X}}$ has almost attained its asymptotic value because no transitions $2\,^3A'' \to X\,^2A''$ take place at large values of R and r. Therefore, further extension of the box will not modify the final probabilities.

Considering the fragmentation along R (and similarly along r), we can estimate the range of R where DE is energetically possible from the PESs and the energy of the incoming electron. As shown in Figure 2, if we call E_K, the kinetic energy gained by the WP on the resonance PES:

$$E_K(R) = E_{e,in} - E_{res}(R) \tag{25}$$

where $E_{e,in}$ is the kinetic energy of the incoming electron. When the system undergoes autoionization to $\tilde{X}\,^2A''$, the maximum energy the emitted electron can take is E_e:
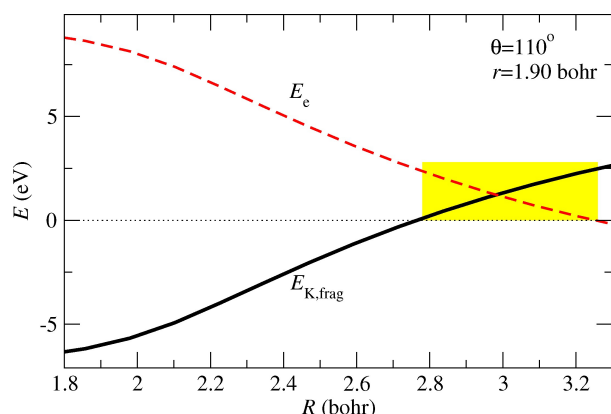
$$E_e(R) = E_{res}(R) - E_{\tilde{X}}(R) \tag{26}$$

which has to be positive. Let us also define the excess energy available for the fragments, $E_{K,frag}$, by the difference between the energy gained by the WP and the energy needed for the fragmentation at the geometry where the autoionization takes place:

$$E_{K,frag}(R) = E_K(R) - [E_{\tilde{X}}(\infty) - E_{\tilde{X}}(R)] \tag{27}$$

Fragmentation of the cation is possible when both E_e and $E_{k,frag}$ are positive. Figure 5 shows that this condition is fulfilled for a very small range of R values, which is consistent with the negligible DE we observe.

A potential limitation of our study is that it only includes one electronic state of the cation. Namely, in the limit $\theta \to 180°$

the states $\tilde{X}\,^2A''$ and $\tilde{A}\,^2A'$ become the two degenerate components of the state $^2\Pi_u$, which leads to a Renner–Teller coupling between these two states. The non-adiabatic transitions $X\,^2A'' \to \tilde{A}\,^2A'$ (and to less extent to $\tilde{C}\,^2A''$) will occur since, as shown in Figure 6, the WP moves to the region of nuclear configurations near $\theta = 180°$. However, our simulation shows that the WP $\Psi_{\tilde{X}}$ does not fragment, which indicates that it is essentially formed by a linear combination of vibrational eigenfunctions with energies below the dissociation threshold. The non-adiabatic transitions will not modify the fragmentation probabilities, since the energy threshold is equal or higher in $\tilde{A}\,^2A'$ than in $\tilde{X}\,^2A''$, and the result shown in Figure 4 for $P_{\tilde{X}}$ can be understood as the probability to find the system in any of the two lowest electronic states of the cation.

Finally, additional mechanisms, not considered in the present simulation, would involve non-adiabatic transitions from the resonant state to resonant states that constitute the Rydberg series that converge to the cation $\tilde{B}\,^2A'$ or $\tilde{A}\,^2A'$ states. The decay of these long-live resonances into the vibrational continuum of H_2O ($\tilde{X}\,^1A'$) would lead to DR (sharp peaks), while their autoionization into cation states could contribute to the DE process. However, we do not expect significant transitions from $2\,^3A''$ to these resonances because it requires changes in two electrons (the Rydberg and core ones) which, in turn, lead to very narrow avoided crossings that would be traversed diabatically by the WP.

Conclusions

We have carried out a wave-packet simulation on the potential energy surface of a resonant state of H_2O with energy above that of the $\tilde{B}\,^2A'$ threshold at the equilibrium geometry of H_2O^+. The calculation shows a rapid electron detachment with a decay into the state of the cation without fragmentation. Accordingly, the formation of the resonant state studied in this work does not contribute to the dissociative excitation process. For this resonant state, the dissociation takes place at times longer than 20 fs, and the probability of this process contributing to the dissociative recombination is about 38%. Therefore, the formation of this resonant state in electron-H_2O^+ collisions will lead to the fragmentation into radicals, but the calculation does not show the formation of H^+ and OH^+ ions. These ions will be produced via non-resonant dissociative excitation (direct excitation into the vibrational continuum of a cationic state) or through formation of other resonances.

Figure 5. Kinetic energy of the emitted electron (E_e, Eq. (26)) and available for the cation fragmentation ($E_{K,frag}$, Eq. (27)), after autoionization, as a function of the coordinate R, for r and θ fixed to the values indicated in the graph. The yellow box indicates the range of values of R where both energies are positive and dissociative excitation is possible.
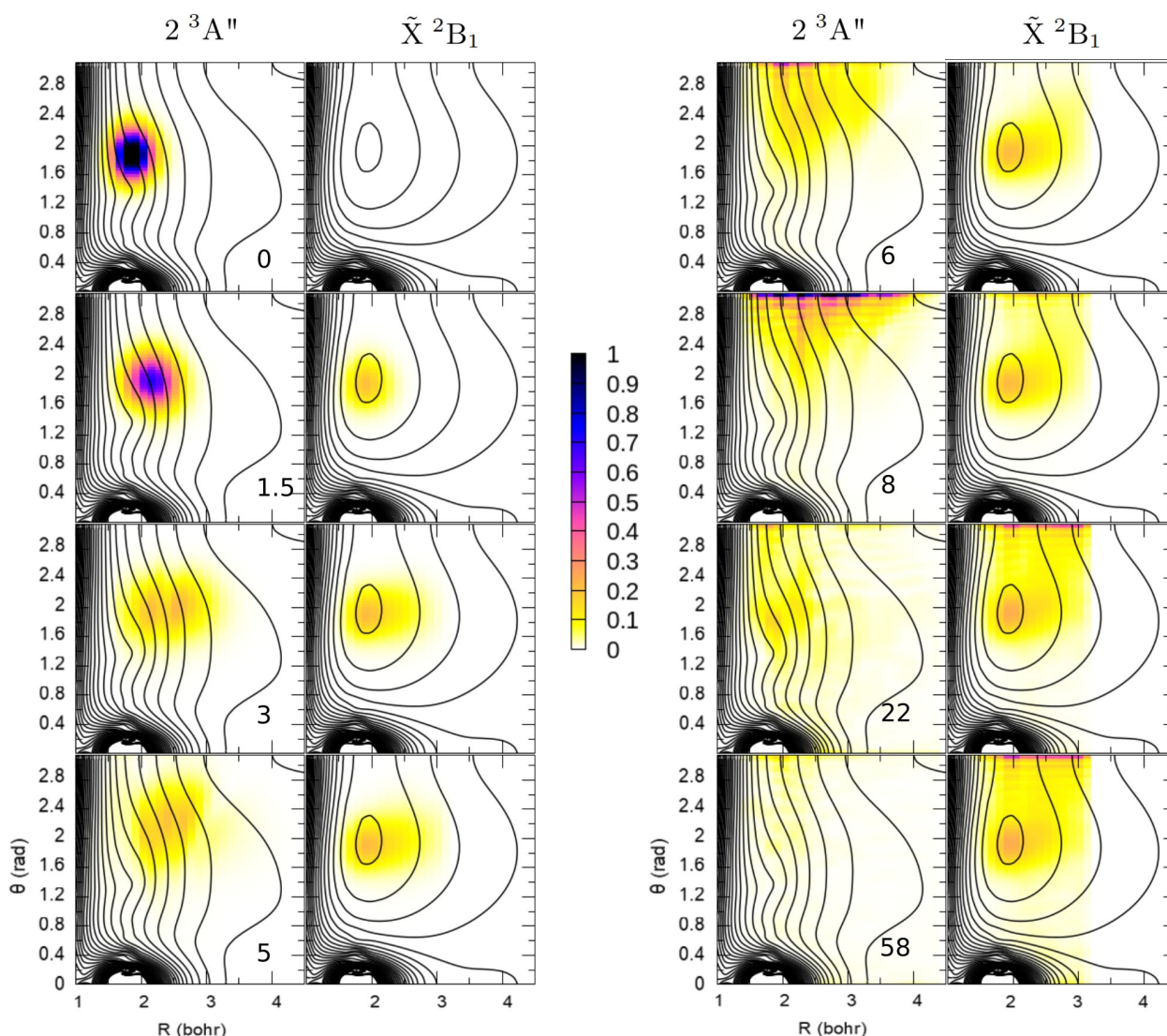
ChemPhysChem

Research Article
doi.org/10.1002/cphc.202300305

Chemistry
Europe
European Chemical
Societies Publishing

Figure 6. Color plot for $r = 1.90$ bohr of the cuts of $|\Psi_{res}|$ and $|\rho_{\tilde{X}}|^{1/2}$ (see Eq. (20)) of the wave packet evolving on the surfaces of the $2\,^3A''$ resonant state (left column of panels in each block) and the cation $\tilde{X}\,^2A''$ (right column of panels in each block), as functions of R and θ (same scale for all the panels) for $t=0$, 1.5, 3, 5, 6, 8, 22, 58 fs, as indicated in the bottom-right corner of the $2\,^3A''$ panels. The wave packets are plotted over the isolines of the corresponding PES. The color scale, common to all panels, is included in the center.

Acknowledgements

Conflict of Interests

The authors declare no conflict of interest.

Data Availability Statement

The data that support the findings of this study are available from the corresponding author upon reasonable request.

[1] M. Dizdaroglu, P. Jaruga, *Free Radical Res.* **2012**, *46*, 382.
[2] M. Jensen, R. Bilodeau, O. Heber, H. Pedersen, C. Safvan, X. Urbain, D. Zajfman, L. Andersen, *Phys. Rev. A* **1999**, *60*, 2970.
[3] P. M. Mul, J. W. McGowan, P. Defrance, J. B. A. Mitchell, *J. Phys. B: At. Mol. Phys.* **1983**, *16*, 3099.
[4] S. Datz, R. Thomas, S. Rosén, M. Larsson, A. M. Derkatch, F. Hellberg, W. van der Zande, *Phys. Rev. Lett.* **2000**, *85*, 5555.

[5] S. Rosén, A. Derkatch, J. Semaniak, A. Neau, A. Al-Khalili, A. Le Padellec, L. Vikor, R. Thomas, H. Danared, M. af Ugglas, M. Larsson, *Faraday Discuss.* **2000**, *115*, 295, https://doi.org/10.1039/a909314a.

[6] R. Thomas, S. Rosén, F. Hellberg, A. Derkatch, M. Larsson, S. Datz, R. Dixon, W. J. van der Zande, *Phys. Rev. A* **2002**, *66*, 032715, https://doi.org/10.1103/PhysRevA.66.032715.

[7] M. Fogle, E. M. Bahati, M. E. Bannister, S. H. M. Deng, C. R. Vane, R. D. Thomas, V. Zhaunerchyk, *Phys. Rev. A* **2010**, *82*, 042720, https://doi.org/10.1103/PhysRevA.82.042720.

[8] S. M. Nkambule, A. Larson, S. Fonseca dos Santos, A. E. Orel, *Phys. Rev. A* **2015**, *92*, 012708, https://doi.org/10.1103/PhysRevA.92.012708.

[9] I. Rabadán, J. Gorfinkiel, *Phys. Rev. A* **2021**, *103*, 032804, https://doi.org/10.1103/PhysRevA.103.032804.

[10] J. Tennyson, *Phys. Rep.* **2010**, *491*, 29.

[11] J. Suárez, L. Méndez, I. Rabadán, *Phys. Chem. Chem. Phys.* **2018**, *20*, 28511.

[12] J. Suárez, L. Méndez, I. Rabadán, *J. Phys. Chem. Lett.* **2015**, *6*, 72.

[13] C. Leforestier, *J. Chem. Phys.* **1991**, *94*, 6388.

[14] R. Guantes, S. C. Farantos, *J. Chem. Phys.* **1999**, *111*, 10827.

[15] J. Suárez, S. C. Farantos, S. Stamatiadis, L. Lathouwers, *Comput. Phys. Commun.* **2009**, *180*, 2025, https://doi.org/10.1016/j.cpc.2009.06.004.

[16] H.-J. Werner, P. J. Knowles, G. Knizia, F. R. Manby, M. Schütz, *Wiley Interdiscip. Rev.: Comput. Mol. Sci.* **2012**, *2*, 242, https://doi.org/10.1002/wcms.82.

[17] Z. Mašín, J. Benda, J. D. Gorfinkiel, A. G. Harvey, J. Tennyson, *Comput. Phys. Commun.* **2020**, *249*, 107092, https://doi.org/10.1016/j.cpc.2019.107092.

[18] H. Tal-Ezer, R. Kosloff, *J. Chem. Phys.* **1984**, *81*, 3967.

[19] C. Leforestier, R. Bisseling, C. Cerjan, M. Feit, R. Friesner, A. Guldberg, A. Hammerich, G. Jolicard, W. Karrlein, H.-D. Meyer, N. Lipkin, O. Roncero, R. Kosloff, *J. Comput. Phys.* **1991**, *94*, 59.

[20] D. Dundas, J. F. McCann, J. S. Parker, K. T. Taylor, *J. Phys. B: At., Mol. Opt. Phys.* **2000**, *33*, 3261.

[21] A. U. Hazi, T. N. Rescigno, M. Kurilla, *Phys. Rev. A* **1981**, *23*, 1089.

[22] C. W. McCurdy, J. L. Turner, *J. Chem. Phys.* **1983**, *78*, 6773.

[23] J. Royal, A. E. Orel, *Phys. Rev. A* **2007**, *75*, 052706, https://doi.org/10.1103/PhysRevA.75.052706.

[24] C. Lanczos, *J. Res. Natl. Bur. Stand.* **1950**, *45*, 255.

Electron capture by H_2O^+ into a resonance just above ist $\tilde{B}$ state sparks a fast elongation of the OH bond while the neutral molecule goes to the linear geometry. The competition between autoionization and dissociation on the potential energy surface of the neutral state determines the proportion of dissociative recombination and dissociative excitation that the system experiences.
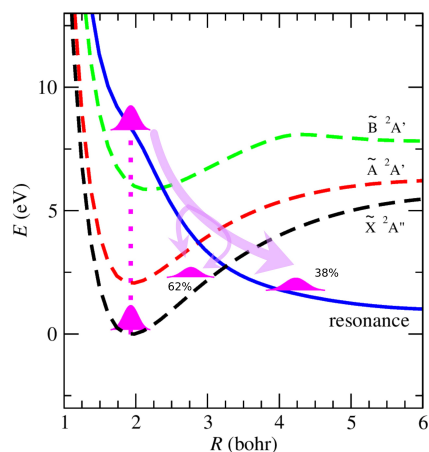
I. Benito-Gómez, Prof. L. Méndez, Dr. J. Suárez, Prof. J. D. Gorfinkiel, Dr. I. Rabadán*

Resonant Fragmentation of the Water Cation by Electron Impact: a Wave-Packet Study